

## CHROMOSOMES

## Structural basis of human telomerase recruitment by TPP1-POT1

Zala Sekne<sup>†</sup>, George E. Ghanim<sup>\*†</sup>, Anne-Marie M. van Roon, Thi Hoang Duong Nguyen<sup>\*</sup>

Telomerase maintains genome stability by extending the 3' telomeric repeats at eukaryotic chromosome ends, thereby counterbalancing progressive loss caused by incomplete genome replication. In mammals, telomerase recruitment to telomeres is mediated by TPP1, which assembles as a heterodimer with POT1. We report structures of DNA-bound telomerase in complex with TPP1 and with TPP1-POT1 at 3.2- and 3.9-angstrom resolution, respectively. Our structures define interactions between telomerase and TPP1-POT1 that are crucial for telomerase recruitment to telomeres. The presence of TPP1-POT1 stabilizes the DNA, revealing an unexpected path by which DNA exits the telomerase active site and a DNA anchor site on telomerase that is important for telomerase processivity. Our findings rationalize extensive prior genetic and biochemical findings and provide a framework for future mechanistic work on telomerase regulation.

**T**elomerase restores telomeric repeats [(TTAGGG)<sub>n</sub> in humans] by de novo DNA synthesis using a telomerase reverse transcriptase (TERT) subunit and an RNA template embedded within telomerase RNA (hTR in humans) (1). Telomerase activity is critical for the long-term proliferation of most cancers and germline and stem cells, whereas telomerase deficiency results in premature aging diseases (2). Human telomerase consists of

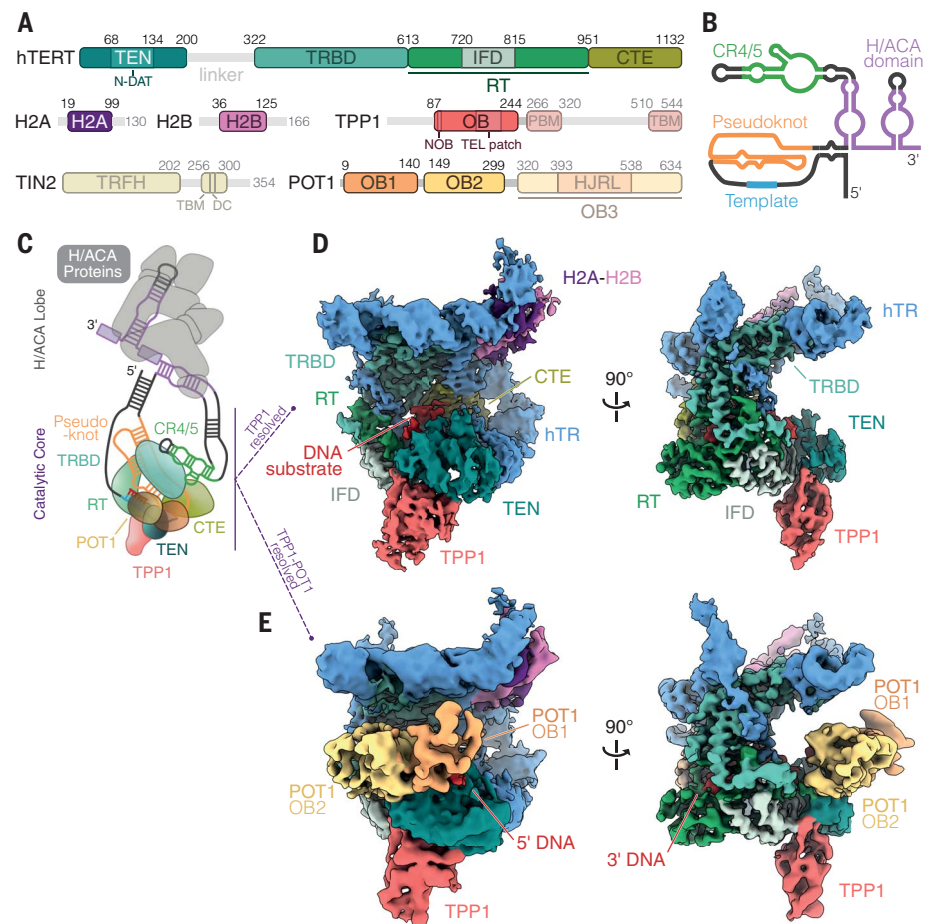
two flexibly tethered functional lobes (3, 4): a catalytic core, in which TERT associates with the pseudoknot/template (PK/t) domain and conserved regions 4 and 5 (CR4/5) of hTR (5), and an H/ACA ribonucleoprotein (RNP) lobe, which is essential for telomerase biogenesis (6) (Fig. 1, A to C). The catalytic core also associates with a histone H2A-H2B dimer (4) (Fig. 1, A, D, and E). Telomerase access to and activity at telomeres is tightly regulated (7). Mam-

malian telomeric DNA is bound and protected by a six-membered protein complex called shelterin (8). The shelterin component TPP1 has been implicated in telomerase recruitment to telomeres (9–13). Within shelterin, TPP1 binds TIN2 and POT1, a single-stranded telomeric DNA binding protein (14, 15). TPP1-POT1 and TPP1-POT1-TIN2 complexes have been demonstrated to stimulate telomerase repeat addition processivity (RAP), which is the ability of telomerase to add multiple telomeric repeats with each DNA binding event (16, 17). Both RAP and interactions with shelterin are essential for telomerase function in vivo (9–11, 18). Yet the structural basis of telomerase-shelterin interactions and shelterin-mediated telomerase processivity remains elusive.

We prepared the human TPP1-POT1-TIN2 (TPT) complex (fig. S1A), demonstrated that it stimulated telomerase processivity in vitro (fig. S1, B and C), reconstituted its complex with human telomerase and the telomeric DNA substrate (T<sub>2</sub>AG<sub>3</sub>)<sub>5</sub> (fig. S1, D and E), and

MRC Laboratory of Molecular Biology, Cambridge CB2 0QH, UK.  
\*Corresponding author. Email: gghanim@mrc-lmb.cam.ac.uk (G.E.G.);  
knguyen@mrc-lmb.cam.ac.uk (T.H.D.N.)  
†These authors contributed equally to this work.

**Fig. 1. Structures of the telomerase catalytic core with telomeric DNA and shelterin components. (A)** Domain organization of protein subunits in the catalytic core and TPT complex. Regions not observed in the structures are displayed as semitransparent. The same domain colors are used throughout, unless indicated otherwise. **(B)** Secondary structure of hTR. **(C)** Schematic of human telomerase bound to TPP1 and POT1. **(D)** A 3.2-Å cryo-EM reconstruction of the telomerase catalytic core-DNA-TPP1 complex (fig. S6). **(E)** A 3.9-Å cryo-EM reconstruction of the telomerase catalytic core-DNA-TPP1-POT1 complex (fig. S7).



verified the retention of the DNA within this complex (fig. S1F). Negative-stain electron microscopy (EM) analyses showed that TPT binds the telomerase catalytic core (fig. S2, A to D). Cryo-EM analyses showed conformational flexibility between the catalytic core, H/ACA lobe, and TPT (figs. S2, E to G; S3; and S4, A to E). Focused classification and refinement resolved the DNA-bound telomerase catalytic core with either TPP1 or TPP1-POT1 at overall resolutions of 3.2 and 3.9 Å, respectively (Fig. 1, D and E; figs. S3 and S5 to S7; and tables S1 and S2). TIN2 could not be resolved by image processing.

In both structures, the TPP1 oligonucleotide/oligosaccharide-binding (OB)-fold domain binds the bottom face of the telomerase catalytic core (Fig. 1, D and E). TERT has four domains: the telomerase essential N-terminal (TEN) domain, the telomerase RNA-binding domain (TRBD), the reverse transcriptase (RT) domain, and the C-terminal extension (CTE) domain (Fig. 1A). TPP1 interposes between the TEN domain and a telomerase-specific insertion in fingers subdomain (IFD) within the RT domain (Fig. 1D, right). In previous structures (3, 4), the TEN domain showed the most conformational variability. TPP1 binding induces conformational changes in the TEN domain and reduces its flexibility, thereby improving its local resolution (figs. S5G and S8A). We also observe a slight compaction of the CTE domain and the P2 stem of hTR (fig. S8, B and D).

The 3.2-Å telomerase-DNA-TPP1 structure reveals the molecular basis of TPP1-telomerase interactions (Fig. 2 and fig. S6, I to K). Previous studies identified an N-terminal region of TPP1 OB-fold domain (NOB) and a TPP1 glutamate and leucine-rich (TEL) patch that are crucial for stimulating telomerase processivity in vitro and telomerase recruitment to telomeres in vivo (fig. S9B) (9–11, 13). The NOB and TEL patch form three areas of contact with TERT (Fig. 2A). The NOB seats into a hydrophobic cleft formed by the TEN domain and the IFD, in contrast to its extended conformation in the crystal structure of the isolated TPP1 OB-fold domain (16) (Fig. 2, B and C, and fig. S6I). The glutamate-rich region of the TEL patch (residues 168 to 172) folds into a short  $\alpha$  helix that is accommodated by a basic surface on the TEN domain (Fig. 2D and fig. S6J). The other region of the TEL patch [residues 210 to 215, Arg<sup>180</sup> (R180), and Leu<sup>183</sup> (L183)] interacts extensively with the TEN domain and IFD (Fig. 2E and fig. S6K). Superimposition of the unbound versus telomerase-bound TPP1 OB-fold structures shows that the TEL-patch loop (residues 212 to 215) has some flexibility to enable interaction with TERT (Fig. 2B). Mutations in the NOB or the TEL patch severely disrupt TPP1-telomerase interactions and recruitment to telomeres (9–11). Thus, the interactions observed here are functionally important for telomerase recruitment by TPP1.

**Fig. 2. Telomerase-TPP1 interactions.** (A) Interactions between the TPP1 OB-fold domain and TERT. The dashed circles indicate the three contacts that the NOB (orange) and TEL patch (red) of TPP1 make with TERT. The  $\beta$  hairpin, which becomes ordered upon TPP1 binding, is highlighted. (B) Comparison of the unbound [gray, PDB ID 2I46 (16)] and telomerase-bound (colored) OB-fold domain of TPP1. (C) Close-up view of the interactions between the NOB of TPP1 and TERT (fig. S6I). (D and E) Close-up views of the interactions between the TEL patch and TERT (fig. S6, J and K). G, Gly; N, Asn; S, Ser; T, Thr. For (C) to (E), the orange dashed lines indicate hydrogen bond and salt bridge interactions.

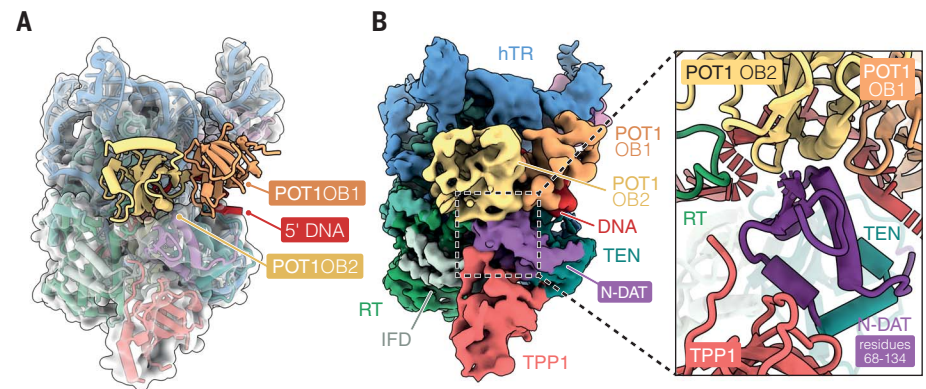
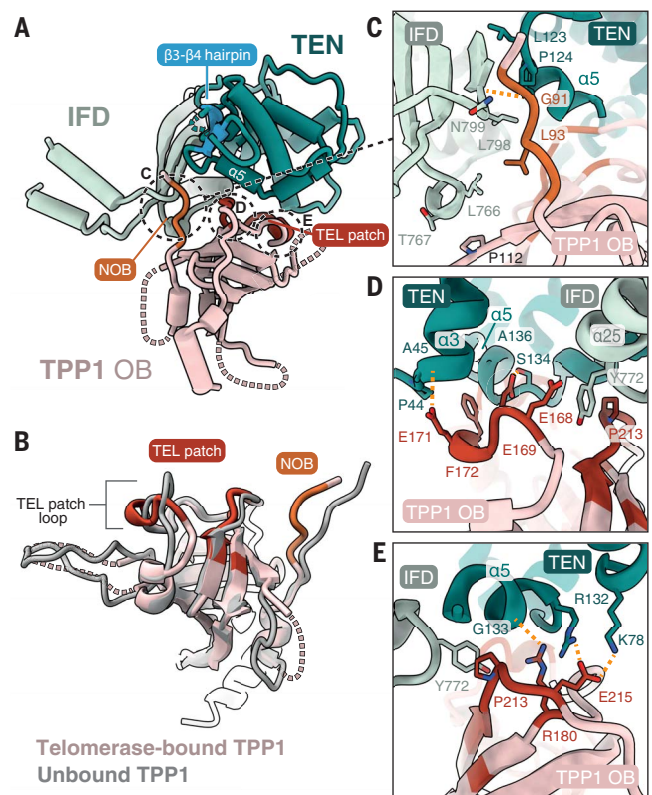


**Fig. 3. Telomerase-POT1 interactions.** (A) Structure of the telomerase-DNA-TPP1-POT1 complex. (B) A 3.9-Å cryo-EM reconstruction of the telomerase-DNA-TPP1-POT1 complex. The inset highlights interactions between POT1 and TERT. The N-DAT region (purple) interacts with both TPP1 and POT1.

Our structure reveals the key TERT regions necessary for TPP1 interaction. Helix  $\alpha 5$  (residues 122 to 135) extensively interacts with TPP1 NOB and the TEL patch (Fig. 2, C to E, and fig. S6, I to K). Upon binding to TPP1, the  $\beta 3$ - $\beta 4$  hairpin and loop 60-76 of TERT become ordered (Fig. 2A and fig. S8A). Both helix  $\alpha 5$  and the  $\beta 3$ - $\beta 4$  hairpin are located in the N-terminal dissociates-of-activities domain of telomerase (N-DAT) that is embedded in the TEN domain (19). Mutations in the N-DAT were shown to have small effects on telomerase catalytic activity but impaired telomere elongation in vivo, suggesting defects in telomerase recruitment to telomeres (19, 20).

Additional contacts were observed between TEN domain Lys<sup>78</sup> (K78), helix  $\alpha 3$  (residues 44 to 46), and the TPP1 TEL patch (Fig. 2, D and E, and fig. S6J). Our findings explain previous studies that showed that charge-reversal mutations at R132 and K78 of the TEN domain substantially reduced the RAP stimulation by TPP1-POT1 and disrupted telomerase localization to telomeres in vivo. These defects were rescued by a charge-swap Glu<sup>215</sup>→Lys (E215K) mutation in TPP1 (12, 21). The IFD has also been suggested to be involved in TPP1 binding and telomerase recruitment to telomeres (22).

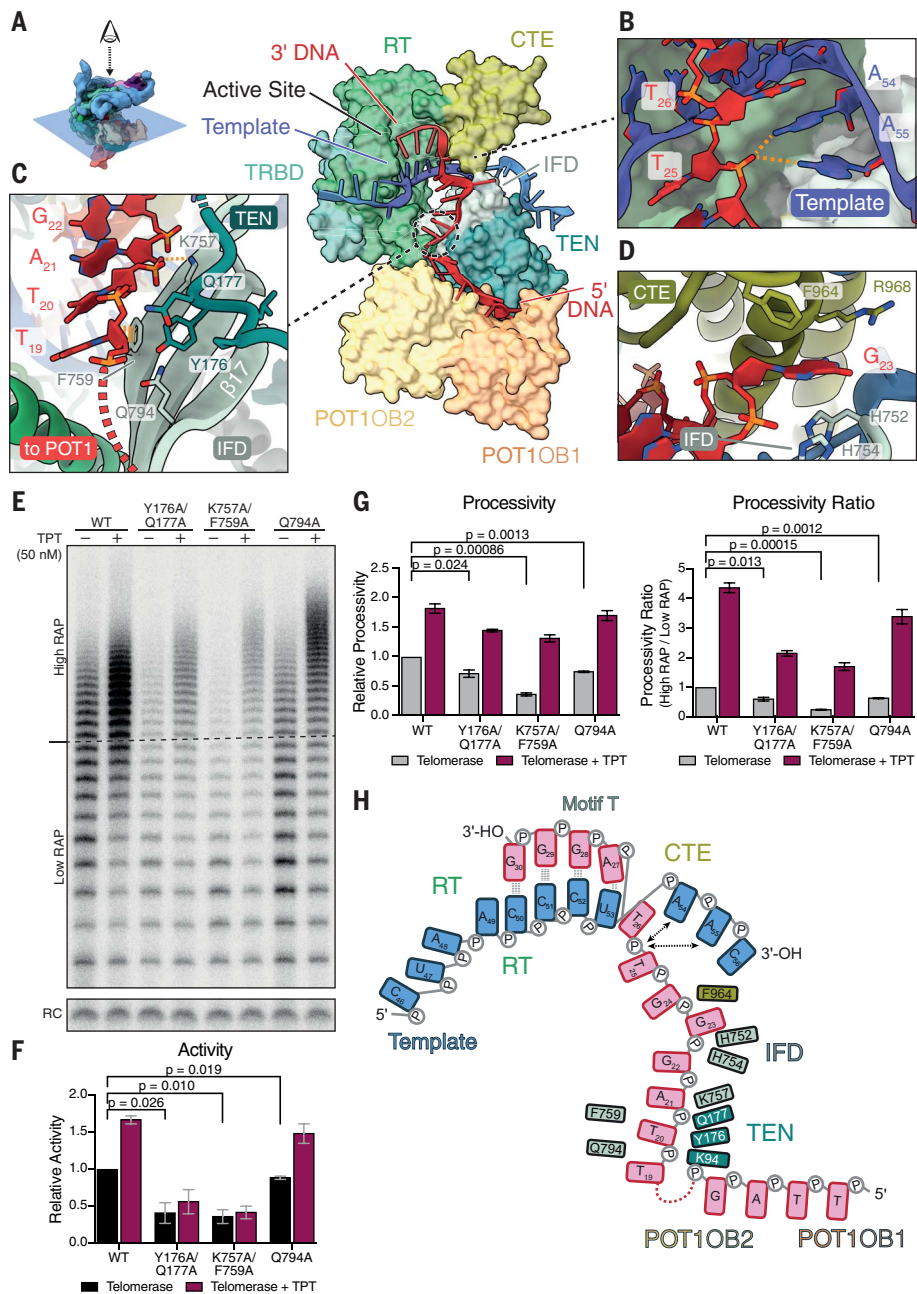


**Fig. 4. Telomeric DNA substrate.** (A) The DNA path guided by TERT, hTR, and POT1. The graphic at the top left shows how the view is related to the telomerase-DNA-TPPI-POT1 reconstruction. (B) Interactions between the template RNA and the DNA upstream of the RNA template-DNA duplex (fig. S6L). For (B) and (C), the orange dashed lines indicate hydrogen bonding and stacking interactions. (C) Close-up view of the interactions between the DNA substrate and the proposed anchor site on the TEN domain and the IFD (fig. S6N). The red dashed line indicates the unmodeled DNA connection. (D) Interactions between the flipped-out G23 DNA base and TERT (fig. S6M). H, His. (E) Telomerase activity assays in the absence and presence of the TPT complex for the wild-type (WT) enzyme and TERT mutants (Y176A/Q177A, K757A/F759A, and Q794A) at the proposed DNA anchor site (fig. S6, H and N). Assays were performed after enzyme enrichment on MagStrepXT resins using ZZ-TEV-twin-Strep-tagged TERT. Experiments were performed in triplicate. Detailed analyses of the input lysates are shown in fig. S12. RC, recovery control. (F and G) Bar graphs showing the quantifications of telomerase activity and processivity of the activity assays shown in (E), respectively. Values were normalized to telomerase without TPT. Error bars are the standard errors of the mean obtained from the replicates. (H) Schematic of the DNA substrate and its interactions with TERT, hTR, and POT1. Only interactions with the 5' part of the DNA following the DNA-RNA duplex are highlighted because interactions of the DNA-RNA duplex with TERT have been discussed previously (4). P, phosphate.

In our structure, the base of an extended  $\beta$  sheet formed by the IFD (residues 766, 767, and 797 to 799) and the TEN domain hold the NOB in place (Fig. 2C and fig. S6I). Additionally, part of the IFD helix  $\alpha 25$  (residues 771 to 775) is sandwiched between the two contact sites in the TEL patch (Fig. 2D).

POT1 is more flexibly engaged with telomerase than TPPI, which is evident from its local resolution range of 7 to 9 Å (figs. S4, C and D, and S5H). The 3.9-Å telomerase-DNA-TPPI-POT1 map allowed us to rigid-body fit a DNA-bound POT1 crystal structure (POT1 OB1 and OB2) (Figs. 1, A and E, and 3; and figs. S7F and S9C) (23). OB3 and the Holliday-junction resolvase-like (HJRL) domains of POT1 and the C-terminal region of TPPI, which interacts with TIN2 and POT1, are unresolved in our structures (Fig. 1A) (24, 25). With high affinity for single-stranded DNA (23), POT1 was thought to associate with telomerase via TPPI and enhance telomerase RAP by increasing avidity to telomeric DNA (16, 26, 27). Surprisingly, POT1 binds not only the DNA substrate but also TERT and forms a gate in front of the telomerase active site (Fig. 3). The N-DAT within the TEN domain wedges between the two OB-fold domains of POT1 (Fig. 3B). Substitutions of POT1-contacting residues in the N-DAT severely affect telomere elongation in vivo with minimal effects on telomerase catalytic activity in vitro (19). Thus, the identified interactions between POT1 and telomerase in our structure are crucial for telomerase recruitment to telomeres in vivo.

We previously used a  $T_{12}(T_2AG_3)$  DNA substrate and observed only the 3' terminal TTAGGG repeat (4). Here, we used a longer  $(T_2AG_3)_5$  DNA substrate to allow for TPPI-POT1 binding. Unlike its ciliate TEBP $\beta$  homolog (28), TPPI does not contact the DNA (fig. S10). Yet its association with telomerase stabilizes the DNA, allowing us to resolve another TTAGGG repeat in our 3.2-Å telomerase-DNA-TPPI map (fig. S6G). The telomerase-DNA-TPPI-POT1 map shows additional DNA density, forming a continuous path between the 12-nucleotide modeled DNA and the DNA bound to POT1 from the previous crystal structure [Protein Data Bank (PDB) ID 1XJV] (23) (fig. S7K). Although the resolution of this region is insufficient for de novo modeling, we use this density and the two DNA models to propose the DNA path through telomerase. The DNA 5' end threads through a positively charged tunnel formed by the POT1 OB1 domain and the TEN domain and is guided along the TEN domain by the POT1 OB2 domain (Fig. 4, A and H, and fig. S11, A and B). The DNA then makes a sharp turn and traverses the IFD and CTE domains before reaching the telomerase active site (Fig. 4A and figs. S6G and S7G).

The telomeric DNA path reveals a previously undiscovered DNA threading surface on

the TEN domain and the IFD of TERT, with implications for telomerase processivity. The TEN domain is essential for RAP and telomerase recruitment to telomeres (12, 29, 30). Several studies have suggested that the TEN domain contains an anchor site that binds the single-stranded DNA substrate and prevents DNA dissociation, thereby promoting RAP (20, 30–34). However, the molecular determinants for the DNA binding activity of the TEN domain and the location of the anchor site remained unclear. We identified a Pro-Leu-Tyr-Gln (PLYQ) motif in the TEN domain (residues 174 to 177), which binds and turns the DNA substrate toward the TEN-POT1 interface (Fig. 4C and figs. S6N, S7I, and S1I, A and B). This motif is highly conserved in vertebrates (fig. S9A). Binding of the TEN domain to the DNA is assisted by the IFD (Q794 and  $\beta$ 17, residues 752 to 759) (Fig. 4C).

To test the role of the PLYQ motif and the IFD as contributors to the DNA anchor site, we reconstituted telomerase with TERT Y176A/Q177A, K757A/F759A, and Q794A mutations (where A is Ala and F is Phe), which significantly reduced telomerase activity and RAP (Fig. 4, E to G, and fig. S12). Addition of the TPT complex rescued the RAP defects in these mutants (Fig. 4, E to G). Similar observations were made previously with Y176A and Q177A single mutations (10, 26, 30). Substitutions at TERT residues 170 to 175 considerably increase the Michaelis constant ( $K_m$ ) for the (T<sub>2</sub>AG<sub>3</sub>)<sub>3</sub> primer and affect telomere elongation in vivo (19, 30). This suggests that the RAP defect observed in the mutants is caused by DNA binding defects during repeat synthesis, and the TPT complex rescued the RAP defects by compensating for the reduced DNA affinity. Thus, we propose that the PLYQ motif of the TEN domain and strand  $\beta$ 17 of the IFD form the anchor site that is crucial for DNA retention during RAP.

hTR also contributes to shaping the DNA path. Immediately downstream of the 4-base pair DNA-RNA template duplex, the RNA template base A54 stabilizes the flipped-out DNA base T26 by base-stacking and coordinates the phosphate backbone of the neighboring T25 together with the RNA template base A55 (Fig. 4, A, B, and H, and fig. S6L). Previous studies showed that the RNA template mutants A54U and A55U compromised telomerase RAP (18), suggesting that these unexpected DNA-RNA template interactions may be important for RAP. We also observe another flipped-out DNA base (G23), which is stabilized by the IFD and CTE domain (Fig. 4, D and H, and fig. S6M).

The *Tetrahymena* p50-TEB complex is functionally comparable to human TPP1-POT1. Whereas TPP1-POT1 is part of the shelterin complex that resides at mammalian telomeres, the p50-TEB complex is part of the *Tetrahymena*

telomerase holoenzyme (35, 36). In *Tetrahymena* telomerase (36), p50 occupies a similar position to TPP1 relative to the TEN domain (fig. S11E). However, POT1 arrangement is notably different from that of TEB (fig. S11E). The DNA substrate in *Tetrahymena* does not travel along the TEN domain as observed in our structure (fig. S11E). The positive charge of the DNA threading surface on the human TEN domain is not conserved in *Tetrahymena* and *Saccharomyces cerevisiae* (fig. S1I, C and D). Therefore, the DNA path along the human TEN domain may be vertebrate specific.

Finally, our structures explain how TPP1 and POT1 facilitate telomerase association with telomeric DNA and stimulate telomerase RAP. With each round of telomeric repeat synthesis, the product DNA can either realign with the template for another round of repeat synthesis or dissociate. In the telomerase structure alone (4), the TEN domain is conformationally flexible, resulting in unstable DNA binding and increased DNA dissociation during repeat synthesis and thus lower RAP (fig. S13A). TPP1 binding stabilizes the TEN domain and allows the anchor site to engage the DNA substrate more stably. POT1 further stabilizes DNA binding by promoting the DNA-TEN domain interaction. Together, TPP1 and POT1 cooperatively increase RAP by reducing DNA dissociation during repeat synthesis, which agrees with previous kinetic studies (37) (fig. S13B). The observed flexibility of POT1 may be necessary for efficient translocation during RAP and/or for accommodating G-quadruplex structures formed by the telomeric DNA product (27) (fig. S4F). Recruitment by shelterin (via TPP1-POT1) would ensure high processivity of telomere-engaged telomerase. Telomerase recruited to a telomere without shelterin would dissociate more easily, thus impairing processive DNA synthesis.

#### REFERENCES AND NOTES

1. E. H. Blackburn, K. Collins, *Cold Spring Harb. Perspect. Biol.* **3**, a003558 (2011).
2. B. Bernardes de Jesus, M. A. Blasco, *Trends Genet.* **29**, 513–520 (2013).
3. T. H. D. Nguyen *et al.*, *Nature* **557**, 190–195 (2018).
4. G. E. Gharim *et al.*, *Nature* **593**, 449–453 (2021).
5. T. L. Beattie, W. Zhou, M. O. Robinson, L. Harrington, *Curr. Biol.* **8**, 177–180 (1998).
6. E. D. Egan, K. Collins, *Mol. Cell. Biol.* **32**, 2428–2439 (2012).
7. J. C. Schmidt, T. R. Cech, *Genes Dev.* **29**, 1095–1105 (2015).
8. T. de Lange, *Annu. Rev. Genet.* **52**, 223–247 (2018).
9. J. Nandakumar *et al.*, *Nature* **492**, 285–289 (2012).
10. A. N. Sexton, D. T. Youmans, K. Collins, *J. Biol. Chem.* **287**, 34455–34464 (2012).
11. F. L. Zhong *et al.*, *Cell* **150**, 481–494 (2012).
12. J. C. Schmidt, A. B. Dalby, T. R. Cech, *eLife* **3**, e03563 (2014).
13. S. Grill, V. M. Tesmer, J. Nandakumar, *Cell Rep.* **22**, 1132–1140 (2018).
14. P. Baumann, T. R. Cech, *Science* **292**, 1171–1175 (2001).
15. J. Z. Ye *et al.*, *Genes Dev.* **18**, 1649–1654 (2004).
16. F. Wang *et al.*, *Nature* **445**, 506–510 (2007).
17. A. M. Pike, M. A. Strong, J. P. T. Ouyang, C. W. Greider, *Mol. Cell. Biol.* **39**, e00593–e00518 (2019).

18. R. A. Wu, J. Tam, K. Collins, *EMBO J.* **36**, 1908–1927 (2017).
19. B. N. Armbruster, S. S. R. Banik, C. Guo, A. C. Smith, C. M. Counter, *Mol. Cell. Biol.* **21**, 7775–7786 (2001).
20. D. C. Sealey *et al.*, *Nucleic Acids Res.* **38**, 2019–2035 (2010).
21. J. L. Stern, K. G. Zyner, H. A. Pickett, S. B. Cohen, T. M. Bryan, *Mol. Cell. Biol.* **32**, 2384–2395 (2012).
22. T. W. Chu, Y. D'Souza, C. Autexier, *Mol. Cell. Biol.* **36**, 210–222 (2015).
23. M. Lei, E. R. Podell, T. R. Cech, *Nat. Struct. Mol. Biol.* **11**, 1223–1229 (2004).
24. C. Chen *et al.*, *Nat. Commun.* **8**, 14929 (2017).
25. C. Rice *et al.*, *Nat. Commun.* **8**, 14928 (2017).
26. A. J. Zaugg, E. R. Podell, J. Nandakumar, T. R. Cech, *Genes Dev.* **24**, 613–622 (2010).
27. L. J. Jansson *et al.*, *Proc. Natl. Acad. Sci. U.S.A.* **116**, 9350–9359 (2019).
28. M. P. Horvath, V. L. Schweiker, J. M. Bevilacqua, J. A. Ruggles, S. C. Schultz, *Cell* **95**, 963–974 (1998).
29. A. R. Robart, K. Collins, *Mol. Cell* **42**, 308–318 (2011).
30. J. Jurczyk *et al.*, *Nucleic Acids Res.* **39**, 1774–1788 (2011).
31. H. D. Wyatt, D. A. Lobb, T. L. Beattie, *Mol. Cell. Biol.* **27**, 3226–3240 (2007).
32. N. F. Lue, *J. Biol. Chem.* **280**, 26586–26591 (2005).
33. S. A. Jacobs, E. R. Podell, T. R. Cech, *Nat. Struct. Mol. Biol.* **13**, 218–225 (2006).
34. B. M. Akiyama, J. W. Parks, M. D. Stone, *Nucleic Acids Res.* **43**, 5537–5549 (2015).
35. H. E. Upton, K. Hong, K. Collins, *Mol. Cell. Biol.* **34**, 4200–4212 (2014).
36. Y. He *et al.*, *Nature* **593**, 454–459 (2021).
37. C. M. Latrick, T. R. Cech, *EMBO J.* **29**, 924–933 (2010).

#### ACKNOWLEDGMENTS

We thank the MRC-LMB EM facility staff for access and support of EM sample preparation and data collection; J. Grimmer and T. Darling for maintaining the computing facility; C. Johnson for assisting with biophysical characterization; A. Carter, K. Collins, R. Hegde, D. Rio, and S. Scheres for critical reading of the manuscript; the Nagai, Löwe, Passmore, and Scheres labs for sharing reagents, equipment, and technical advice; B. Greber for sharing a script to calculate conformational changes; D. Barford, K. Collins, E. Nogales, and S. Scheres for their support; T. Croll for advice with ISOLDE; and E. Zhong for advice with CryoDRNG. **Funding:** T.H.D.N. is supported by a UKRI-Medical Research Council grant (MC\_UP\_1201/19). G.E.G. is supported by a Jane Coffin Childs Postdoctoral Fellowship. **Author contributions:** T.H.D.N. initiated and supervised the project. Z.S. and G.E.G. purified samples, prepared EM grids, collected and analyzed EM data, and performed model fitting and all biochemical experiments and quantification. G.E.G. performed model building and refinement. A.-M.M.v.R. prepared telomerase extracts and performed model refinement. Z.S., G.E.G., and T.H.D.N. analyzed the structures. Z.S., G.E.G., A.-M.M.v.R., and T.H.D.N. wrote the paper. **Competing interests:** The authors declare that they have no competing interests. **Data and materials availability:** Cryo-EM maps of telomerase-DNA-TPP1 are deposited with the Electron Microscopy Database under accession numbers EMD-14196 (sharpened) and EMD-14198 (unsharpened). Cryo-EM maps of telomerase-DNA-TPP1-POT1 are deposited with the Electron Microscopy Database under accession numbers EMD-14197 (sharpened) and EMD-14199 (unsharpened). PDB coordinates are deposited with the Protein Data Bank under accession numbers 7QXA for the telomerase-DNA-TPP1 complex, 7QXB ( $\alpha$ -POT1), and 7QXS (POT1 with side chains) for the telomerase-DNA-TPP1-POT1 complex. Materials are available from T.H.D.N. under a material transfer agreement with the MRC-Laboratory of Molecular Biology.

#### SUPPLEMENTARY MATERIALS

science.org/doi/10.1126/science.abn6840  
Materials and Methods  
Figs. S1 to S13  
Tables S1 to S3  
References (38–66)  
MDAR Reproducibility Checklist  
Movies S1 and S2  
Data S1 to S5

[View/request a protocol for this paper from Bio-protocol.](#)

13 December 2021; accepted 7 February 2022  
Published online 24 February 2022  
10.1126/science.abn6840